Pair spectra and the magnetic properties of Mn^{2+} in double nitrate crystals*

R. W. Wilkins† and J. W. Culvahouse
Department of Physics and Astronomy, The University of Kansas, Lawrence, Kansas 66045
(Received 3 December 1975)

Experimental electron-paramagnetic-resonance spectra for Mn^{2+} pairs in $La_2Zn_3(NO_3)_{12}\cdot 24H_2O$ host crystals are interpreted to obtain the exchange interaction, $J\vec{S}_1\cdot\vec{S}_2$, for pairs of ions in nearest-neighbor X and Y sites, $J(X, Y) = 0.0193 \pm 0.001$ cm^{-1}, and for pairs of ions in nearest-neighbor X sites, $J(X, X) = 0.0309 \pm 0.0015$ cm^{-1}. The zero-field splitting parameter D has also been determined for the members of these pairs. For ions in the X site, these values are much different than for the isolated ions. The information obtained for isolated pairs is used as an aid in the interpretation of measurements on the concentrated crystal $La_2Mn_3(NO_3)_{12}\cdot 24H_2O$ reported by other authors. From this analysis, a plausible magnetic ordering arrangement is found for the concentrated material below its magnetic critical point. It is concluded from a comparison of calculated and measured magnetothermal properties that the magnetic interactions are the same in the concentrated material as for isolated pairs within the quoted accuracy of the latter. From the trends of the zero-field splitting for ions in the Y site as the diamagnetic constituents are varied, it is deduced that $D = -0.0209$ cm^{-1} for ions in the Y site of the concentrated material. The anisotropy of the ^{55}Mn γ rays from magnetically ordered $La_2Mn_3(NO_3)_{12}\cdot 24H_2O$ observed by other authors is utilized to obtain a best value for the zero-field splitting of ions in the X site, $D = -0.0090$ cm^{-1}. The magnitude of $J(X, Y)$ determined by the experiments agrees very well with an earlier estimate made by Francis and Culvahouse based on measurements of the magnetic interactions of other ions in these sites and a model in which only e_g orbitals are involved in the exchange. The value obtained for $J(X, X)$ reenforces the conclusion advanced earlier on the basis of measurements for other ions that the exchange between ions in nearest-neighbor X sites involves both ferromagnetic and antiferromagnetic interactions.

I. INTRODUCTION

For several years we have been engaged in the measurement by means of electron paramagnetic resonance (EPR) of the magnetic interactions of isolated pairs of iron-group magnetic ions hosted in diamagnetic isomorphs of magnetic hydrated crystals. The purpose of this work is to provide a basis for understanding the origins of magnetic interactions between hydrated magnetic complexes, and to explicate the low-temperature cooperative phenomena of the concentrated crystals.

Significant progress has been made toward the development of a semiempirical theory for the exchange interactions between the divalent iron-group ions in $La_2Zn_3(NO_3)_{12}\cdot 24H_2O$ (LaZnN). Earlier work on Co pairs,[1,2] on Ni pairs,[3] and on a number of mixed pairs[4] has appeared to justify simplifying approximations in the description of the magnetic interactions between one type of near-neighbor pair (the X-Y pairs) that lead to a concise and satisfying description in terms of an antiferromagnetic exchange between a single pair of d orbitals. For the other type of near-neighbor pair (the X-X pairs), data thus far indicate that essentially all orbitals are involved in the exchange and that many of these constituent interactions are ferromagnetic. Because Mn^{2+} has a full complement of half-occupied d orbitals, the interactions of pairs of Mn^{2+} ions in LaZnN provide a critical test of the theory of the X-Y interactions and very valuable information on the nature of the more complex X-X interaction.

The determination of the Mn^{2+} interactions has been inhibited by the extreme complexity of the pair spectra. Recently, we have completed a facility for computer-assisted EPR spectroscopy[5] which greatly improves the quality of data which we can obtain and facilitates the comparison of observed spectra with the predictions of models. Aside from the importance of the interpretation of the Mn^{2+} for understanding exchange interactions, the present analysis has served as an initial test of the power of our version of computer-assisted EPR spectroscopy.

Sections II and III of this paper treat the analysis of the spectra of Mn pairs. In Sec. V pair results are compared with measurements on LaMnN and a model for the ordered state of LaMnN is developed and compared with the experimental results of Mess *et al.*[6]

II. ANTICIPATIONS BASED ON THEORY AND EXPERIMENT

A. Anticipated form of the magnetic interactions

The rhombohedral unit cell of cerium magnesium double nitrate (CeMgN) has been determined by Zalkin *et al.*,[7] and the positions of the near-neighbor (nn) divalent ions have been tabulated and depicted by Culvahouse and Schinke.[1] The unit

cell contains two divalent ions in X sites and one in a Y site. Each X site has a nn X site 4.99 Å away along the c (trigonal) axis, and three nn Y sites 7.14 Å away and at an angle of 62.7° from the c axis. The magnetic interactions between these pairs have been designated the X-X and X-Y interactions and were the only interactions found to be significantly different from dipolar for pairs of Co^{2+} and Ni^{2+}.[1,3] We provisionally assume that this is true for Mn^{2+} pairs as well. Mn^{2+} has no orbital angular momentum in its ground-state configuration; the excited configurations lie at very high energies; and the exchange interactions will be weak. These observations justify the assumption that the nondipolar spin-spin interaction will be isotropic and bilinear. The dipolar interaction is assumed to be that of dipoles with $g=2.002$ located at the positions of the Mg^{2+} ions determined by Zalkin. Experience with other divalent pairs suggests that this assumption about the spatial relationship of the ions will lead to errors of less than 3%, but the large size of the Mn^{2+} ion *vis à vis* Mg^{2+} might lead to somewhat larger errors.

For the nn X-X pairs the interaction is assumed to have the form

$$\mathcal{H}_{12}(X,X) = J(X,X)(\vec{S}_1 \cdot \vec{S}_2) - 2J^{(d)}(X,X)[S_{1z}S_{2z} - \tfrac{1}{2}(S_{1x}S_{2x} + S_{1y}S_{2y})], \quad (1)$$

where z is the c axis and

$$J^{(d)}(X,X)/g\mu_B = g\mu_B/R^3 = 148 \text{ G}, \quad (2)$$

where R is the interionic separation.

Upon inserting numerical values for the angular factors, the X-Y interaction has the form

$$\begin{aligned}\mathcal{H}_{12}(X,Y) &= J(X,Y)(\vec{S}_1 \cdot \vec{S}_2) \\ &+ 2J^{(d)}(X,Y)\{0.185[S_{1z}S_{2z} - \tfrac{1}{2}(S_{1x}S_{2x} + S_{1y}S_{2y})] \\ &- 0.612(S_{1z}S_{2x} + S_{1x}S_{2z}) \\ &- 0.592(S_{1x}S_{2x} - S_{1y}S_{2y})\},\end{aligned} \quad (3)$$

where the x axis is in the plane of the c axis and the interionic axis, and

$$J^{(d)}(X,Y)/g\mu_B = 50.9 \text{ G}. \quad (4)$$

For a field in the direction of the trigonal axis, all X-Y pairs are equivalent.

The interpretation of the pair spectra has also been facilitated by the availability of estimates of the order of magnitude of the exchange interactions. Francis and Culvahouse[4] have estimated $J(X,Y) = 0.0191$ cm^{-1} from measurements on mixed pairs and the simplified theory of the X-Y interaction. Using this value for $J(X,Y)$, the measurements on LaMnN discussed in Sec. IV can be used to estimate that $J(X,X)$ lies in the range 0.01–0.05 cm^{-1}.

B. Spin Hamiltonian of isolated ions

If Z is understood to designate either the X or Y site, the form of the isolated ion spin Hamiltonian in traditional notation is[8]

$$\begin{aligned}\mathcal{H}(Z) &= g\mu_B \vec{H} \cdot \vec{S} + A\vec{I} \cdot \vec{S} + D(Z)(S_z^2 - \tfrac{35}{12}) \\ &+ \tfrac{7}{36}[F(Z) - a(Z)](S_z^4 - \tfrac{95}{14}S_z^2 + \tfrac{81}{16}) \\ &+ (\tfrac{1}{36}a(Z)\sqrt{2})[(S_zS_+^3 + S_+^3S_z)e^{3i[\varphi+\varphi(Z)]} \\ &+ (S_zS_-^3 + S_-^3S_z)e^{-3i[\varphi+\varphi(Z)]}].\end{aligned} \quad (5)$$

The z axis is the trigonal axis, the effective spin S is the ionic spin and is $\frac{5}{2}$. The spin I of the 100% abundant ^{55}Mn is also $\frac{5}{2}$. The values of g and A are 2.002 and -0.00900 ± 0.00005 cm^{-1} for both sites and are independent of temperature and the cation constituents of the host crystal.

The value of D is very different for the two sites and is sensitive to temperature and the cation constituents of the host crystal. Because the spectra are sensitive to the values of D, it is important to establish approximate limits on the values of D that will be found for the pairs. The values of D and $a-F$ for a number of situations are tabulated in Table I. The relative insensitivity of the Y site parameters to temperature and constituents illustrated by the values in Table I has been noted for Ni and Co as well.[1,3] It has also been noted for Ni and Co pairs, that more strain is produced at an X site by a misfitting ion in the nn X site than is produced by a misfitting ion in the nn Y site. Since Mn^{2+} is a larger ion than Zn^{2+}, we approached the analysis of the pair spectra with the assumption that $D(Y)$ of an X-Y pair would not differ by more than 10% from that for isolated Y ions in LaZnN, and that $D(X)$ of an X-Y pair would not differ by more than 30% from that for isolated X ions in LaZnN. For $D(X)$ in X-X pairs we were prepared for larger variations. Table II contains the values which we have determined for the pairs. Roughly, the measured values correspond to the expected variations although the value of $D(X)$ for X-X and X-Y pairs were both somewhat beyond the anticipated limits.

Possible variations of a-F are not very important and in all of the calculations on the pairs this parameter has been left fixed at 7×10^{-4} cm^{-1} for both the X and Y ions in all pairs. For lanthanum magnesium double nitrate (LaMgN) at room temperature Van Ormondt[9] finds $F(X) = 0.28\times10^{-4}$ cm^{-1} and $F(Y) = 1.54\times10^{-4}$ cm^{-1}. The phase angle

TABLE I. Spin-Hamiltonian parameters for Mn^{2+} for a number of situations.

Host	Situation	Temperature (K)	10^4D (cm^{-1})	$10^4(a-F)$ (cm^{-1})	Reference
			X site		
LaMg*N*	Isolated	296	+21.0 ± 0.4	+8.8 ± 0.4	a
LaHg*N*	Isolated	77.4	−40.1 ± 0.3	+9.6 ± 0.3	a
LaHg*N*	Isolated	4.2	−49.4 ± 0.3	+9.7 ± 0.3	a
LaZn*N*	Isolated	77.4	−62.6 ± 0.5	+9.0 ± 1	b
LaZn*N*	Isolated	4.2	−70.3 ± 0.5	+9.0 ± 1	b
BiMg*N*	Isolated	90	−64 ± 1	+10 ± 1	c
BiMg*N*	Isolated	20	−80 ± 1	+10 ± 1	c
LaZn*N*	Mn(*X*)-Mn(*Y*) prs.	4.2	−93 ± 2	···	d
LaZn*N*	Mn(*X*)-Mn(*X*) prs.	4.2	−131 ± 1	···	d
LaMn*N*	Concentrated	4.2	−90 ±	···	d
			Y site		
LaMg*N*	Isolated	296	−188.6 ± 0.4	+7.3 ± 0.4	a
LaMg*N*	Isolated	77.4	−218.3 ± 0.2	+8.0 ± 0.3	a
LaMg*N*	Isolated	4.2	−220.1 ± 0.3	+8.1 ± 0.3	a
LaZn*N*	Isolated	77.4	−210.0 ± 0.5	+9 ± 1	b
LaZn*N*	Isolated	4.2	−212.0 ± 0.5	+7 ± 1	b
BiMg*N*	Isolated	90	−211 ± 1	+8 ± 1	c
BiMg*N*	Isolated	20	−215 ± 1	+8 ± 1	c
LaZn*N*	Co(*X*)-Mn(*Y*) prs.	4.2	−211 ± 2	···	e
LaZn*N*	Mn(*X*)-Mn(*Y*) prs.	4.2	−209 ± 2	···	d
LaMn*N*	Concentrated	4.2	−209		d

[a] B. M. Brandt, D. Van Ormondt, and T. Thalhammer, Phys. Lett. 19, 549 (1965); and Ref. 9.
[b] J. W. Culvahouse (unpublished).
[c] R. S. Trenam, Proc. Phys. Soc. Lond. A 66, 118 (1953).
[d] This work.
[e] C. L. Francis and J. W. Culvahouse (unpublished).

$\varphi(Z)$ was found to correspond to directions within a few degrees of the projection of the metal-ion–oxygen bonds onto a plane perpendicular to the *c* axis. This fine detail is of no importance for fitting pair spectra with the field along the *c* axis but may be significant in the detailed characterization of the ordered state.

In the analysis of the pair spectra we have to contend with the variation of five important parameters, $D(X)$ of an *X*-*X* pair, $D(X)$ and $D(Y)$ of an *X*-*Y* pair, $J(X,X)$, and $J(X,Y)$. The limitation on the ranges of variation for these parameters established in this section were very important in defining the type of perturbation scheme suitable for the evaluation of models.

III. PAIR SPECTRA AND THEIR INTERPRETATION

A. Experimental spectra

For a field applied along the symmetry axis, each type of isolated Mn^{2+} ion produces an EPR spectrum consisting of five nearly equally spaced sets of six nearly equally spaced hyperfine components. The spectra are centered very near the field $H_0 = h\nu/g\mu_B$, where ν is the spectrometer frequency. Except for second-order hyperfine effects ($\sim A^2/g\mu_B H$), the hyperfine components are spaced by approximately $2D(X)/g\mu_B = 149$ G, and the *Y*-ion sets are spaced by approximately $2D(Y)/g\mu_B = 456$ G. For $\nu = 16.52$ GHz, the result is 60 lines between 4960 and 7060 G. The outermost *Y*-

TABLE II. Spin-Hamiltonian parameters for *X*-*X* and *X*-*Y* pairs in $La_2Zn_3(NO_3)_{12}\cdot 24H_2O$.

Pairs	J (cm^{-1})	$D(X)$ (cm^{-1})	$D(Y)$ (cm^{-1})
X-*X*	0.0309 ± 0.0015	−0.0131 ± 0.0002	···
X-*Y*	0.0193 ± 0.0010	−0.0093 ± 0.0005	−0.0209 ± 0.0004

ion transitions ($M=\pm\frac{5}{2}\rightarrow M=\pm\frac{3}{2}$) lie approximately 480 G outside of the corresponding X-ion transitions.

The pair spectra are expected to be complex. A qualitative analysis based on the anticipated pair parameters predicts several thousand lines of significant intensity near and within the isolated ion spectra. Figures 1(a) and 1(b) depict the realization of this complexity. The absorption spectra shown there are for the ranges of approximately 1000 G above and 1000 G below the outermost lines of the spectrum of the isolated Y ions. The spectra were taken at a temperature of 1.2 K, using a microwave frequency of 16.52 GHz, and with the field along the c axis of LaZnN crystal with 1% of the Zn replaced by Mn.

In the analysis of complex pairs, absorption spectra are much more valuable than derivative of absorption spectra, because the closeness of agreement between experimental and synthesized spectra is much easier to judge. The spectra shown in Fig. 1 are the result of signal averaging for 20 up and down sweeps of the magnetic field at a rate of 1 cycle every 2 min. The magnet control and the digitization of the output of a superheterodyne reflection-type spectrometer are carried out by instrument modules of a system called the Digital Instrumentation Node.[10] The Digital Instrumentation Node is also interfaced with a ModComp II/5 computer where the data are averaged and higher level control of the experiment is exercised. The averaged data are packaged in a form which facilitates convenient retrieval and stored on the disk memory of a larger ModComp II/5 computer which serves as the "Hub" of the Chemical Physics Computer Network. The data and synthesized spectra are displayed on a Tektronix 4010 graphics unit interfaced with the laboratory computer. Hard copy is obtained remotely at the Hub computer, and the more extensive calculations required in real time are also performed in the Hub because of its greater computational speed and core size. Some details of the system have been given by Wilkins *et al.*[11]

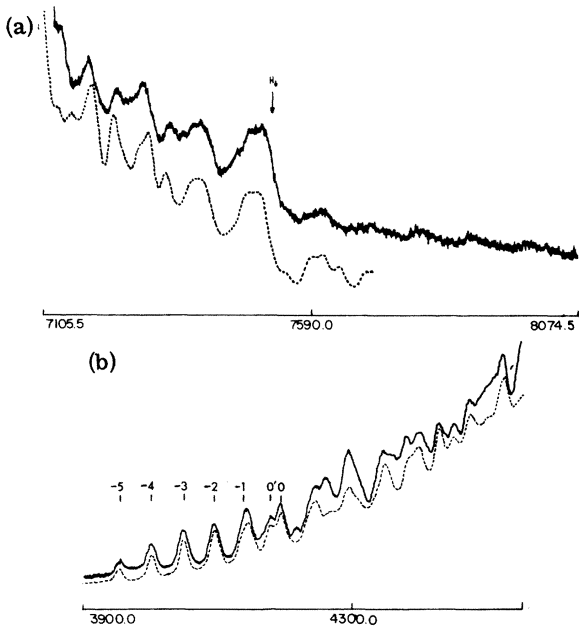

FIG. 1. (a) Mn-Mn pair spectrum above the isolated ion spectrum for an applied field parallel to the c axis, at a temperature of 1.2 K, and observing frequency of 16.52 GHz. The solid line is the experimental absorption spectrum. The dashed line is the spectrum calculated for the following pair parameters: For X-Y pairs, $D(Y)=-0.0209$ cm^{-1}, $D(X)=-0.0093$ cm^{-1}, $J(X,Y)=0.0193$ cm^{-1}. The rms linewidth for individual lines was taken to be 8.5 G. The contribution of the X-X pairs to this spectrum is insignificant. (b) The Mn-Mn pair spectrum below the isolated ion spectrum for the same conditions as in (a). The solid line is the experimental spectrum. The lines designated by numbers are discussed in the body of the paper. The dashed line is the spectrum calculated for the following pair parameters: For X-Y pairs, the same as in (a). For X-X pairs, $D(X)=-0.0131$ cm^{-1}, $J(X,X)=0.0336$ cm^{-1}. The rms linewidth of the X-X pair lines was taken to be 5.5 G. The contribution of X-Y pairs to this spectrum is not large.

Despite the complexity of the spectra there are two striking features which proved to be keys to a successful interpretation. First, in the low-field spectrum of Fig. 1(b) there is a series of lines labeled −5, −4, −3, −2, and −1 which are spaced by approximately $\frac{1}{2}A$ and increase in intensity from −5 to −1 in a nearly stepwise fashion. This is the pattern expected for the hyperfine structure of pairs of identical ions coupled by an isotropic exchange interaction larger than the hyperfine interaction.[2,12] The second feature occurs in the high-field spectrum at a field H_4 which is marked in Fig. 1(a) with an arrow, where the intensity of the pair spectra abruptly rises. The implications are not so immediately obvious for this second feature but it has proved helpful in the determination of the parameters for the X-Y pairs. The first feature has obvious implications for the interpretation of the X-X pair spectra to which we turn in Sec. III B.

B. Approximate interpretation of the low-field spectra

For a field along the c axis, the complete X-X pair Hamiltonian may be written

$$\begin{aligned}\mathcal{H}_{12}^{(T)} &= g\mu_B H(S_{1z}+S_{2z}) + D(X)(S_{1z}+S_{2z})^2 \\ &\quad + J_e \vec{S}_1\cdot\vec{S}_2 + (\tfrac{1}{2}A)(\vec{I}_1+\vec{I}_2)\cdot(\vec{S}_1+\vec{S}_2) \\ &\quad - [2D(X)+3J^{(d)}(X,X)]S_{1z}S_{2z} + B_4^0[O_4^0(S_1)+O_4^0(S_2)] \\ &\quad + (\tfrac{1}{2}A)(\vec{I}_1-\vec{I}_2)\cdot(\vec{S}_1-\vec{S}_2), \end{aligned} \tag{6}$$

where

$$J_e = J(X,X) + J^{(d)}(X,X), \tag{7}$$

and the notation $B_4^0 O_4^0$ has been introduced for the fourth-rank spin tensor.[13] The first four terms are diagonal in a representation which diagonalizes the total electronic spin S_T and the total nuclear spin I_T. If the effect of the transverse hyperfine interactions can be ignored, the projections of the total electronic and nuclear spins on the z axis, M_T and m_T, are separately good quantum numbers. The sixth term has diagonal elements in the S_T, M_T representation and also couples states differing by 2 and 4 in S_T. Fortunately the nondiagonal effects of this term will be negligible because of the small value for B_4^0. The fifth term has diagonal elements and couples states differing by 2 in S_T; but while its magnitude may be comparable to or larger than J_e, it has no effect on the states with $M_T = \pm 5$ and ± 4 which are expected to be the levels which give rise to the outermost lines in the spectrum. The last term couples states differing by 1 in S_T, and is antisymmetric in the nuclear spin.

Ignoring the last three terms and the transverse components of the fourth term, each electronic transition with $\Delta M_T = \pm 1$, will exhibit an eleven-line hyperfine structure with an interval $\frac{1}{2}A$ and a stepwise increase in intensity from the extreme lines ($m_T = \pm 2I$) to the center line ($m_T = 0$) which is suggestive of the behavior of the low-field pair lines discussed in Sec. II.

For the X-Y pairs one does not expect such a simple hyperfine structure because of the large difference in $D(X)$ and $D(Y)$. The Hamiltonian for X-Y pairs can be cast into the form (6) with $D(X)$ replaced by $\overline{D} = \frac{1}{2}[D(X) + D(Y)]$ and one additional term

$$\mathcal{H}_{12}^{(AS)} = \tfrac{1}{2}[D(X) - D(Y)](S_{1z}^2 - S_{2z}^2). \tag{8}$$

If this term were sufficiently large in comparison with the exchange term, the spin-spin interaction could be treated by a simple local-field approximation and the spectra would consist of single-ion spectra of the X and Y ions shifted in field. For the anticipated range of parameters this term will only destroy the approximation of a diagonal S_T, and a complex intermediate case with complicated hyperfine structure will be realized.

We conclude from this preliminary analysis that the low-field lines -5 to -1 in Fig. 1(b) are due to X-X pairs. In the approximation used thus far, the lines are either the $5, -5$ to $5, -4$ or the $5, 5$ to $5, 4$ transitions and are located at

$$H = H_0 \pm [4D(X) - 7.5J^{(d)}(X,X)] \mp (\tfrac{1}{2}A)m_T. \tag{9}$$

At a temperature of 1.2 K and a field of 5000 G, the -5 to -4 transition is expected to be 150 times stronger than the 5 to 4 transition because of the low population of the higher-lying levels. Since only the low-field lines can be seen at this temperature, we conclude that $D(X)$ is negative, and approximately -0.0135 cm^{-1}. The 1.2-K spectra were chosen for display in Fig. 1 because they emphasize these important lines. At higher temperatures, these low-field lines become weaker relative to the remainder of the pair spectra.

In the approximation that has been used, the spectra identified above are not sensitive to J_e. However, the $5, -4$ and the $4, -4$ levels are separated by only $5J_e$ and the last term in (6) which couples these levels may have a significant effect. If one continues to ignore terms of the order of $A/g\mu_B H$, this last term can be treated exactly for the $M_T = -4$ levels. The result is the following correction to Eq. (9)

$$\Delta H = -\mathrm{sgn}(J_e)(\tfrac{1}{2}|A|)\{[(5J_e/2A)^2 + (m_1 - m_2)^2]^{1/2} - 5|J_e/A|\}. \tag{10}$$

The implications of an analogous formula for ions with electronic spin of $\frac{1}{2}$ has been discussed in detail elsewhere.[2] These corrections split the component lines of the stair-step pattern, the largest effect occurring for the center line of the pattern because it contains transitions corresponding to the largest values of $m_1 - m_2$. It appears that the lines -5 to -1 are progressively broadened by these effects; that the line 0′ corresponds to transitions for which $m_1 - m_2 = \pm 5$, and the line 0 is a composite of the other $m_T = 0$ transitions. This interpretation of the 14.5-G separation of 0 and 0′ yields $J_e = -5A = 0.045$ cm^{-1} or $J(X,X) = 0.03$ cm^{-1}. This result must be accepted with reserve because the shift involved is of the same magnitude as the second-order effects of the transverse components of the hyperfine structure.[14] The final determination is discussed in Sec. III D.

C. High-field pair spectrum

The preliminary analysis for the X-X pairs implies that at 1.2 K there can be only very minor contributions to the high-field spectrum from these pairs, and the major features must emerge from solution of the X-Y pair Hamiltonian. The only possible approach to this part of the problem is a purely numerical one involving the diagonalization of many matrices and the examination of synthesized spectra obtained by superposing lines at the calculated field positions. If the transverse hyperfine correction is ignored, M_T is a good quantum number, and the calculation of the eigenvalues and eigenvectors of the Hamiltonian can be reduced to the diagonalization of many matrices of dimension $6 - |M_T|$ in the product representation,

$|S_1M_1\rangle|S_2M_2\rangle|I_1m_1\rangle|I_2m_2\rangle$.

A computer program was written which calculated these matrices and diagonalized them for each value of M_T and each nuclear spin product state. The energy difference between levels with $\Delta M_T = \pm 1$ were calculated for all possible combinations. Since the energy differences vary linearly with magnetic field in this approximation, it was possible to select those pairs of energy levels which gave lines in the field region of immediate interest. For these selected transitions, the transition matrix elements were calculated from the wave functions produced by the diagonalization process (representation R_1), and the square of this matrix element was weighted by the thermal occupation probability for the lowest level involved in the transition. If this intensity was greater than 1% of the intensity of the strongest transition found in the region of interest, it was saved and the second-order hyperfine corrections were applied to the transition using the representation R_1. The most significant defect in this procedure is that it does not allow for possible near or exact degeneracies which require the more elaborate considerations discussed in the appendix. The maximum errors from this defect are of the order of 2 or 3 G and will not affect very many transitions.

Using parameters in the anticipated range, crude spectral plots were first generated on a teletype terminal of The University of Kansas time sharing computer system. About 100 such plots were examined. It was found that the sharp increase in intensity as one approaches the isolated-ion spectra from high field, was always observed although it varied in sharpness. It was found that the field position at which this increase occurred was very insensitive to $D(X)$, but that it was sensitive to $D(Y)$ and $J(X, Y)$ according to the relation

$$\delta H_{\downarrow} = -4.0[\delta D(Y)] + 1.5[\delta J(X, Y)]. \qquad (11)$$

This feature is produced by a few of the $M_T = -2$ to $M_T = -1$ transitions, and examination of the wave functions for these states reveal that the transition is almost purely a $-\frac{5}{2}$ to $-\frac{3}{2}$ transition of a Y ion which accounts for the variation with $D(Y)$. The variation with $J(X, Y)$ is not accounted for by a simple picture of the local field cast by the X ion.

If we assume that the D value for the Y-ion member of the pair is that for isolated ions, Eq. (11) implies $J(X, Y) = 0.020$ cm^{-1}. Other features of the spectra are sensitive to variations of $D(Y)$ and $J(X, Y)$ constrained by Eq. (11) and of $D(X)$. This sensitivity has been used to obtain independently determined values for all three parameters.

In the final optimization of the fit, the large computer program described above was iterated four times to find the rate of changes of position for all significant lines with respect to variations of $D(Y)$, $D(X)$, and $J(X, Y)$. These numbers were used in the laboratory computer to synthesize spectra which were compared with the experimental spectra on the Tektronix graphics terminal. At this stage in the analysis, the small contributions of the X-X pairs to the high-field spectrum were included using the best preliminary estimates for the X-X parameters.

The analysis was concluded with the fit shown in Fig. 1(a) obtained with the spin-Hamiltonian parameters listed in Table II. The synthesized spectra includes contributions from ~400 lines and a separately adjusted quadratic baseline intended to allow for the tail of the isolated-ion spectrum. The rms linewidth used for the synthesized spectra is 8.5 G, 50% larger than that for the isolated-ion spectra. The larger linewidth is thought to be needed to compensate for the small errors in the treatment of the second-order hyperfine corrections and possible lack of alignment of the field along the c axis ($\pm 1°$) which would split the spectra of the three types of X-Y pairs. Changes of 0.5% in $J(X, Y)$ compensated by changes in $D(Y)$ to keep $H_{\downarrow}$ fixed produce significant changes in the synthesized spectra as do changes of 1% in $D(X)$.

D. Refinement of the interpretation of the low-field spectrum

Using exactly the same process as that described for the high-field spectra, the synthesized spectra shown in Fig. 1(b) were obtained for $J(X,X) = 0.0336$ cm^{-1} and $D(X) = -0.0131$ cm^{-1}. The lower part of the spectrum is dominated by the X-X contributions. The synthesized spectrum contains contributions from ~600 lines and a separately adjusted quadratic baseline. The linewidth used in the synthesized spectrum was chosen on the basis of the sharpness of the peak 0, and is the same as the width for the isolated spectrum. The value of $J(X,X)$ was chosen to fit the $0 - 0'$ separation.

In the upper-half of the spectra there are minor discrepancies which may arise partly from the imprecise representation of the X-Y contributions which may be judged from the quality of fit for the high-field spectra; but more likely from a compounding of small errors in the calculated X-X spectrum which are already apparent in the low-field portion. In Fig. 2, the low-field spectrum is expanded to make these defects more apparent. These errors are due to the treatment of the second-order hyperfine corrections in a product representation for the nuclei. In view of the importance of the splitting $0 - 0'$ in the determination of $J(X,X)$, a synthesized spectrum was calcu-

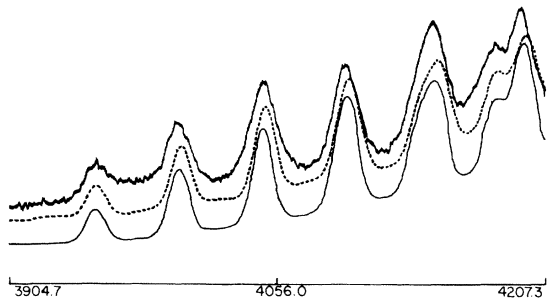

FIG. 2. Comparison of the lowest portion of the low-field pair spectrum with calculations using two different approximations. The upper solid line is the experimental spectrum. The dashed line is the calculated spectrum shown in Fig. 1(b). The lower solid line is a spectrum for the X-X pairs alone calculated as described in the Appendix of this paper with $J(X,X)=0.0309$ cm^{-1}.

lated for the lowest seven peaks using the formulation described in the Appendix which deals accurately with the problems induced by degeneracy, but is only second order in the correction due to the antisymmetric part of the hyperfine interaction. The results for this calculation using $J(X,X)=0.0309$ cm^{-1} is also depicted in Fig. 2. The shape of the calculated spectrum is in better consonance with the experimental spectrum, and we have taken this value of $J(X,X)$ as the best experimental value (see Table II).

IV. COMPARISON OF PAIR RESULTS WITH THE PROPERTIES OF LANTHANUM MANGANESE DOUBLE NITRATE

The temperature dependence of the isothermal susceptibility, the magnetic specific heat, and the ordering energy of lanthanum manganese double nitrate (LaMnN) are primarily determined by the exchange interactions, but the zero-field splittings D and the dipolar interactions have a significant influence. For initial comparison with experimental results, we assume that the exchange interactions are those listed in Table II; that $D(Y)$ in LaMnN has the value found for the Y ion of X-Y pairs; and that $D(X)$ has the value found for X-X pairs. This last assumption is the one most in doubt and in comparing our predictions with observations on the directional distribution of γ rays emitted by ^{55}Mn in ordered LaMnN, we arrive at a better value for $D(X)$ in LaMnN which is used in the final comparison of the predictions of pair data with observations.

A. Isothermal susceptibility

The isothermal susceptibility can be expressed as a power series in the reciprocal of the temperature

$$\chi_{\beta\beta}=\alpha_{\beta\beta}+\frac{C_{\beta\beta}}{T}\left(1+\frac{\Theta^{(1)}_{\beta\beta}}{T}+\frac{\Theta^{(2)}_{\beta\beta}}{T^2}+\cdots\right), \quad (12)$$

in which each of the coefficients in the temperature-dependent part is defined by traces of $\mathcal{H}^n S_\beta H_\beta$, where $\mathcal{H}$ and S are, respectively, the total Hamiltonian and spin and H is the applied field. For $\Theta^{(1)}_{\beta\beta}$, one finds contributions from the dipolar interaction, the zero-field splittings, and the exchange interaction so that for fields parallel and perpendicular to the symmetry axis

$$\Theta^{(1)}_{\parallel}=\Theta^{(1)}_e+\Theta^{(1)}_d+\Theta^{(1)}_D, \quad (13)$$

$$\Theta^{(1)}_{\perp}=\Theta^{(1)}_e-\tfrac{1}{2}(\Theta^{(1)}_d+\Theta^{(1)}_D), \quad (14)$$

where

$$\Theta^{(1)}_d=\frac{2S(S+1)g^2\mu_B^2}{3kN}\sum_{i>j}\frac{3z_{ij}^2-r_{ij}^2}{r_{ij}^5}, \quad (15)$$

$$\Theta^{(1)}_D=\{-[4S(S+1)-3]/45k\}[2D(X)+D(Y)], \quad (16)$$

and

$$\Theta^{(1)}_e=[-2S(S+1)/9k][J(X,X)+6J(X,Y)]. \quad (17)$$

For the lattice parameters given by Zalkin *et al.*, we find[15]

$$\frac{1}{N}\sum_{i>j}\frac{3z_{ij}^2-r_{ij}^2}{r_{ij}^5}=3.761\times10^{21}\ \text{cm}^{-1}. \quad (18)$$

Using the values selected at the beginning of this section for the spin-Hamiltonian parameters we find

$$\Theta^{(1)}_d=5.50\times10^{-2}\ \text{K},\quad \Theta^{(1)}_D=4.82\times10^{-2}\ \text{K},$$

$$\Theta^{(1)}_e=-0.412\ \text{K}.$$

Nelson and Sapp[16] have reported the results of fitting measurements of the isothermal susceptibility between 1.2 and 4.2 K to the Curie-Weiss formula

$$\chi_{\beta\beta}=\alpha_{\beta\beta}+C_{\beta\beta}/(T-\Theta_{\beta\beta}). \quad (19)$$

The results are tabulated in the first row of Table III. Assuming that $\Theta_{\beta\beta}$ can be identified with $\Theta^{(1)}_{\beta\beta}$, these results agree very well with the values calculated from the pair interactions which are listed in the last row of Table III. Results from similar

TABLE III. Measured and calculated values for the Curie-Weiss temperatures of $La_2Mn_3(NO_3)_{12}\cdot24H_2O$.

	$\Theta_{\parallel}$	$\Theta_{\perp}$	$\Theta_{\parallel}-\Theta_{\perp}$	Θ_e
Calc.	−0.309	−0.465	0.115	−0.412
Ref. 16	−0.306 ± 0.011	−0.486 ± 0.017	0.18	−0.426
Ref. 6	−0.47	−0.42	−0.05	−0.44

measurements by Mess *et al.*[6] are listed in the second row of Table III. For these measurements, the anisotropy of the susceptibility is severely discordant with the other results.

There is considerable uncertainty in the constants determined from isothermal susceptibility measurements. Wolf and Heintz[17] have demonstrated that the constants obtained in fitting susceptibilities are strongly dependent on the number of terms in the fitting polynomial. Use of the Curie-Weiss law corresponds to an unjustified constraint on the higher-order terms of (12). Sapp[18] has reanalyzed the Nelson-Sapp data using a power series of the form of (12). He finds that the value of $\Theta_e^{(1)}$ varies between -0.368 and -0.242 as the number of constants in the polynomial and the weighting of the experimental points are varied. He finds a much smaller variation in $\Theta_{\parallel}^{(1)} - \Theta_{\perp}^{(1)}$. Our conclusion is that excellent fits to the experimental data are given by $\Theta_e^{(1)} = -0.35 \pm 0.010$ K; but the data are a weak test for the validity of our pair-interaction data for LaMnN.

B. Magnetic specific heat

For temperatures well above the Néel temperature (0.230 K for LaMnN [6]) the magnetic specific heat per gram-ion is given by the first term obtained using a high-temperature expansion of the density matrix

$$C/R = b/T^2 . \tag{20}$$

There are contributions to b from the dipolar interaction, the zero-field splitting, the exchange interaction, and the hyperfine interaction:

$$b_d = \frac{2S^2(S+1)^2}{3}\left(\frac{g^2\mu_B^2}{k}\right)^2 \frac{1}{N}\sum_{i>j}\frac{1}{r_{ij}^6} , \tag{21}$$

$$b_D = \frac{S(S+1)[4S(S+1)-3]}{135k^2}\{2[D(X)]^2+[D(Y)]^2\} , \tag{22}$$

$$b_e = \frac{S^2(S+1)^2}{9k^2}\{[J(X,Y)]^2+6[J(X,Y)]^2\} , \tag{23}$$

and

$$b_n = S(S+1)I(I+1)/3k^2A^2 . \tag{24}$$

For the Zalkin lattice

$$\frac{1}{N}\sum_{i>j}\frac{1}{r_{ij}^6} = 4.463\times10^{41}\ \text{cm}^{-6} . \tag{25}$$

Inserting this dipole sum and our assumed values for the other parameters we find in units of K^2: $b_d = 1.43\times10^{-2}$, $b_D = 3.35\times10^{-3}$, $b_e = 5.65\times10^{-2}$, $b_n = 4.28\times10^{-3}$, and for the sum of all of these

$$b = 0.0784\ K^2 . \tag{26}$$

Nelson and Sapp[18] have measured the ratio of the adiabatic to isothermal susceptibility at 4.2 K in a wide range of applied fields using the Casimir-Dupre formulation. They report $b = 0.070 \pm 0.002$ K^2. The results depend very slightly on the assumed temperature dependence of the isothermal susceptibility, and in conjunction with his reevaluation of the isothermal susceptibility data, Sapp has found

$$b = 0.073 \pm 0.002\ K^2 , \tag{27}$$

which is in reasonable agreement with our calculated value.

Mess *et al.*[6] have also determined b by fitting the calorimetric specific heat between 0.35 and 0.60 K to Eq. (20), obtaining $b = 0.060$ K^2. This fit is not over a large range and not at sufficiently high temperatures that higher-order terms in the expansion of the density matrix are completely negligible. We therefore accept the value obtained by Sapp in this and in later comparisons.

C. Ordered state of lanthanum manganese double nitrate

1. Plausible ordering arrangements

The exchange interactions in LaMnN couple Mn ions lying in adjacent layers perpendicular to the c axis. The Y-ion layers are spaced at intervals of 11.53 Å along the c axis and are coupled only by very weak dipolar interactions. Two X-ion layers 3.27 Å above and below the Y-ion layer are strongly coupled to the Y-ion layer by the X-Y interactions. This interaction is dominated by antiferromagnetic exchange and will result in ferrimagnetic X-Y-X sandwiches. The X-X interactions couple adjacent sandwiches. The isotropic exchange component of the X-X interaction is antiferromagnetic and favors an antiparallel arrangement of adjacent sandwiches which would produce an over-all antiferromagnetic structure. The very strong anisotropic dipolar component of the X-X interaction favors a parallel ordering of the sandwiches if they are ordered along the c axis. In the case of lanthanum nickel double nitrate (LaNiN) the X-X exchange interaction is ferromagnetic and a ferrimagnetic structure is the most stable one. In the present case, the antiferromagnetic X-X exchange is sufficiently strong that the antiferromagnetic structure is the most stable, but the dipolar interaction has two important effects. First it causes the ferrimagnetic pattern which we shall refer to as the F structure to be only marginally higher in energy than the antiferromagnetic or A structure. Secondly, the dipolar X-X interaction reduces the anisotropy energy of the A structure to such a low value that rather refined calculations are required to predict the direction of the ordering axis which produces minimum energy.

2. First-order calculations

In this subsection we present the results of molecular-field calculations of the ordering energy for the A and F structure. We also refer to this calculation as a first-order calculation in the sense of quantum-mechanical perturbation theory because it amounts to calculating the diagonal components of the total magnetic Hamiltonian in a representation that is a product of states of the individual ions with extremal projections ($\pm\frac{5}{2}$) of the ionic spin on the ordering axis z'. The Hamiltonian for the system is written

$$\mathcal{H} = \sum_i \left(\mathcal{H}_i + \sum_j \tfrac{1}{2}\mathcal{H}_{ij} \right), \tag{28}$$

in which $\mathcal{H}_i$ is the isolated ion Hamiltonian for the ion at site i and $\mathcal{H}_{ij}$ the pair interactions. The contribution of all interactions except those of nn X-X and X-Y are referred to as the distant dipolar interactions, and their effects were calculated by a direct summation of the z' component of the local field at each type of site for all "distant" ions within a radius of 150 Å. The contribution to the ordering energy from the distant interactions is

$$\frac{E_{\rm dd}}{R} = \begin{cases} -0.0097 P_2(\cos\theta), & A \text{ structure} \\ -0.0293 P_2(\cos\theta), & F \text{ structure} \end{cases} \tag{29}$$

where θ is the angle of the ordering axis from the c axis and $P_2(\cos\theta)$ is the unnormalized Legendre polynomial. The sign convention used is such that more stable structures have a more positive ordering energy.

For the F structure, the distant dipolar interactions also lead to a demagnetization field and a corresponding addition to the ordering energy

$$E_{\rm df}/R = -0.002\,13[df(\theta) - \tfrac{4}{3}\pi], \tag{30}$$

where $df(\theta)$ is the demagnetization factor of the sample.

The first-order contributions from the single-ion terms are the same for the A and F structures

$$\begin{aligned} E_{\rm SI}^{(1)}/R = {} & (10/9k)[2D(X) + D(Y)] P_2(\cos\theta) \\ & + (0.0040) P_4(\cos\theta) \\ & + (8.28\times 10^{-7}) P_4^3(\cos\theta)\cos 3[\varphi - \varphi(X)], \end{aligned} \tag{31}$$

where the last two terms which arise from the fourth-rank crystal-field terms have been numerically evaluated using parameters given in Sec. II. The nn spin-spin interactions yield

$$\begin{aligned} E_{\rm nn}^{(1)}/R = {} & (25/12k)[6J(X,Y) \pm J(X,X)] \\ & + (25/6k)[(1.11)J^{(d)}(X,Y) \\ & \mp J^{(d)}(X,X)] P_2(\cos\theta), \end{aligned} \tag{32}$$

where the upper and lower signs apply for A and F, respectively.

Using the standard parameters suggested at the beginning of this section, we find for all first-order terms except the small fourth-rank terms in (31)

$$E^{(1)}/R = 0.441 + 0.0167 P_2(\cos\theta)$$

for the A structure, and

$$\begin{aligned} E^{(1)}/R = {} & 0.256 - 0.002\,13[df(\theta) - \tfrac{4}{3}\pi] \\ & + 0.1621 P_2(\cos\theta) \end{aligned}$$

for the F structure.

3. Second-order corrections to the ordering energy

The energy of the ground state g is lowered further by the coupling to excited states e through the off-diagonal elements of the Hamiltonian. This results in an increase in the ordering energy

$$E^{(2)} = \sum_e \frac{|\langle e|\mathcal{H}|g\rangle|^2}{E_e}, \tag{33}$$

where E_e is the excitation energy for excited state e.

For an ordering direction along the c axis, the most important second-order contributions for both A and F structures are from the transverse components of the nn X-Y interaction. For the A structure there is a nearly equally important contribution from the transverse components of the nn X-X pairs. The total effects for all terms are

$$\frac{E^{(2)}}{R}(0) = \begin{cases} 0.0360, & A \text{ structure} \\ 0.0103, & F \text{ structure}. \end{cases} \tag{34}$$

For ordering directions not along the c axis the second-order corrections have a complex angular dependence which may be quite significant for the A structure. The most important of these off-axis contributions arises from the terms

$$\sin\theta\cos\theta \sum_{X-\text{ion pairs}} \Big([\tfrac{1}{2}D(X)](S_{1-}S_{1z} + S_{1+}S_{1z} + S_{2-}S_{2z} + S_{2+}S_{2z}) + \tfrac{3}{2}J^{(d)}(X,X)[(S_{1+} + S_{1-})S_{2z} + S_{1z}(S_{2+} + S_{2-})] + 0.555 \sum_{\text{nn } Y \text{ ions}} (S_{1+} + S_{1-} + S_{2+} + S_{2-})S_{iz} \Big)$$

in the spin Hamiltonian which couples the ground state to the single X-ion excitations. The result is a contribution to the second-order ordering energy which is a maximum at 45° if the angular dependence of the excitation energy is ignored and the magnitude of which is quite sensitive to the value of $D(X)$. When this term becomes sufficiently large, the minimum ordering energy occurs in a direction away from the c axis. Careful calculations including all terms in (28) and the angular variation of the excitation energies show that the c axis is the preferred direction for $D(X) < -0.0116$, but for more positive D values, the direction of preferred orientation swings rapidly toward a direction 45° from the c axis. The angle for the maximum ordering energy and the value of the ordering energy is shown in Table IV for a number of values for $D(X)$ which are in the range of plausibility.

4. *Comparison with experimental results*

Mess *et al.*[6] have calculated the total ordering energy of LaMnN from specific-heat measurements between 0.08 and 0.55 K. They obtain $0.437R$ per gram-ion, but $0.109R$ of this is obtained by extrapolation of the specific heat above 0.55 K using Eq. (20) with $b = 0.060$ K^2. If one uses instead Sapp's value for b, an ordering energy of $0.469R$ is obtained, which is in reasonable agreement with the values in Table IV.

Results which are very significant for our model have been obtained by Mess *et al.* from a study of the γ-ray emission from ^{54}Mn nuclei in LaMnN at 0.048 K. Calculations in Sec. IV C 3 lead to the result that the Mn spins in the ground state of the A structure have approximately 95% of their maximum spin projections on the ordering axis and the lowest-lying excited states are about 0.30 K above the ground state. This situation should produce a nuclear orientation almost identical to the orientation calculated for the Mn in pure $\pm\frac{5}{2}$ states. Instead Mess *et al.* find that the anisotropy of the γ rays is only 60% of this maximum value in zero applied field. A field of 500 G along the c axis produces the maximum orientation for the experimental temperature.

TABLE IV. Calculated ordering energy and the angle θ_1 of the ordering axis relative to the c axis for $La_2Mn_3(NO_3)_{12} \cdot 24H_2O$ for several values of $D(X)$.

$D(X)$ (cm^{-1})	E_{ord}/R (K)	θ_1 (deg)
−0.0131	0.493	0.0
−0.0116	0.489	0.0
−0.0104	0.486	21.5
−0.0090	0.485	30.0
−0.0083	0.484	33.0

The anisotropy of the γ rays in zero applied field can be explained by assuming that LaMnN orders in antiferromagnetic domains that are tilted from the c axis. We assume that there will be three directions of minimum energy, at an angle θ_1 with the c axis and at three azimuthal angles $\varphi(X)$ $(\mathrm{mod}\frac{2}{3}\pi)$. For this model the relative γ-ray emission rates along the c axis and perpendicular to it will be given by

$$W(0) = 1 - \tfrac{1}{2}A_2(3\cos^2\theta_1 - 1) \tag{35}$$

and

$$W(90) = 1 - \tfrac{1}{2}A_2(\tfrac{3}{2}\sin^2\theta_1 - 1), \tag{36}$$

where $A_2 = 0.15$ and we have neglected a small term arising from the 4th-rank statistical tensor for the Mn nuclei (f_4). If we take $\theta_1 = 31°$, we find $W(0) = 0.91$ and $W(90) = 1.045$ in satisfactory agreement with the experiments. In our model, this angle for the domain axes would be realized for $D(X) = -0.0090$ cm^{-1} which we have listed in Table I as the best value of the $D(X)$ for LaMnN.

Some aspects of the field dependence remain difficult to explain. In an applied field, the domains would be expected to rotate continuously (in the case of domains tilted from the c axis there is no flopping) until the domains are perpendicular to the field. We can calculate from our anisotropy energies and the experimental susceptibilities that a field of the order of 500 G would produce a significant change in the domain orientation, and would tend to reduce the difference between $W(0)$ and $W(90)$, whereas there appears to be an increase in the difference for modest fields.

The fact that the full anisotropy is observed in fields greater than 500 G applied along the c axis may be explained by the small energy difference between the F structure and the A structure. Even for the slab geometry which was used in the nuclear orientation experiment, our results predict that the F structure will be lowest for a field of 740 ±160 G along the c axis.

The change in the nuclear orientation observed for parallel fields between 2500 and 4500 G appears to be related to the cancellation of the internal field at the Y ions by the applied field. For a slab geometry and the F structure the internal field is approximately 2900 G. We have not pursued a detailed explanation of the behavior in this range nor that for fields applied perpendicular to the x axis.

D. Summary comparison of pair and bulk data

Data from the three types of bulk measurements discussed in this section have been used to fix

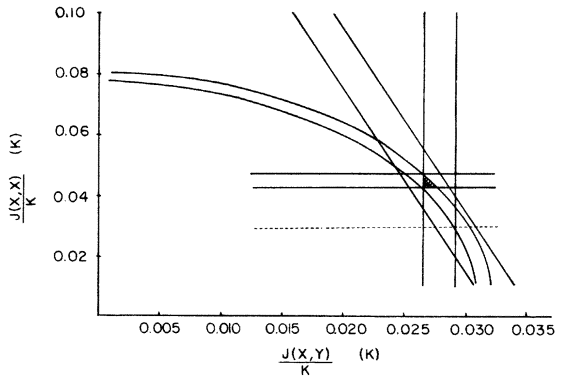

FIG. 3. Constraints imposed on $J(X,Y)$ and $J(X,X)$ by measurements of the magnetic specific-heat tail, and by measurement of the ordering energy are depicted by the two segments of an ellipse, and by two parallel sloping lines. Vertical and horizontal lines represent the limits for isolated pairs. The region of compatibility with all measurements is crosshatched. The dashed horizontal line represents the smallest value of the X-X interaction for which antiferromagnetic ordering should be observed.

relationships between $J(X,X)$ and $J(X,Y)$, some of which are plotted in Fig. 3. Assuming that $\Theta_e^{(1)}$ is -0.35 ± 0.10, we find from Eq. (17)

$$(1/k)[J(X,X)+6J(X,Y)] = 0.180 \pm 0.050 \text{ K}. \quad (37)$$

From the specific-heat data, assuming $D(X) = -0.0090 \text{ cm}^{-1}$, $D(Y) = -0.0209 \text{ cm}^{-1}$, we find from Eqs. (21)–(24)

$$(1/k^2)\{[J(X,X)]^2+6[J(X,Y)]^2\} = (6.11 \pm 0.24)\times 10^{-3} \text{ K}^2. \quad (38)$$

Using the same values for zero-field splittings and assuming an experimental value of $0.469R$ for the ordering energy, we find

$$(1/k)[J(X,X)+6J(X,Y)] = 0.204 \pm 0.010 \text{ K}. \quad (39)$$

The loci of the extreme limits of Eqs. (38) and (39) are plotted in Fig. 3. Equation (37) is not plotted. It is compatible with (38) and has a larger error. Vertical and horizontal lines in the figure correspond to the limits on the experimentally measured pair interactions. There is a region of mutual compatibility; but the bulk measurements do not define $J(X,X)$ very well. However, the observed antiferromagnetic ordered state requires $J(X,X)/k < 0.029$ K. This limit is indicated by the dashed line in Fig. 3.

V. CONCLUSIONS

Our pair measurements and the analysis of measurements on LaMnN lead us to conclude that the pair interactions in LaMnN are the same as those measured for isolated pairs in LaZnN within the fairly large uncertainties which remain for LaMnN. Conclusions reached earlier for LaCoN and LaNiN *vis à vis* isolated pairs suggest that the interactions are the same in LaMnN as in isolated pairs within the experimental errors of the latter. We believe that the spin-Hamiltonian parameters deduced here for LaMnN should provide information required to explain all of the details of susceptibility, nuclear orientation, and magnetocaloric effects in the ordered state of LaMnN. We have pursued some of these effects further than reported here and found promising results, except that, as noted in Sec. IV C, we are puzzled by the behavior of the nuclear orientation for fields of a few hundred gauss applied along the c axis.

The best experimental value for the X-Y exchange interaction is within 1% of the value predicted by Francis and Culvahouse from the systematics of the X-Y interaction in other pairs. The rather large antiferromagnetic interaction for the X-X pairs is qualitatively consistent with the hypothesis advanced earlier[3] that for these pairs, exchange between like orbitals is ferromagnetic and exchange between unlike orbitals is antiferromagnetic.

ACKNOWLEDGMENTS

We wish to thank Dr. R. C. Sapp for his suggestions, and for the use of his results in advance of publication. D. Baldwin, Dr. M. J. Hennessy, and Dr. J. Marple all made invaluable contributions to the hardware development which made the experiments possible.

APPENDIX: EFFECTIVE HYPERFINE INTERACTION HAMILTONIAN FOR EXCHANGE-COUPLED ELECTRON SPINS

Feutchwang[19] developed an effective Hamiltonian for several nuclei coupled to a single electron spin by a hyperfine interaction $AI_zS_z + B(I_xS_x + I_yS_y)$. He showed that the transverse part of the hyperfine interaction leads to an effective interaction between the nuclei of the order of $B^2/g\mu_B H$ which is very important in the analysis of the electron-nuclear double resonance spectra of equivalent nuclei. A somewhat similar effect occurs for nuclei interacting with different electronic spins which are coupled by an electronic exchange interaction. This situation is described by the Hamiltonian

$$\mathcal{H} = g\mu_B \vec{H}\cdot\vec{S} + \tfrac{1}{2}J[S_T(S_T+1) - S_1(S_1+1) - S_2(S_2+1)] + \tfrac{1}{2}A[\vec{I}_T\cdot\vec{S}_T + (\vec{S}_1 - \vec{S}_2)\cdot(\vec{I}_1 - \vec{I}_2)] - g_n\mu_n\vec{H}\cdot\vec{I}_T . \quad \text{(A1)}$$

An effective Hamiltonian for the nuclei is obtained for each electronic state S_T, M_T by calculating the hyperfine interaction to second order in an unspecified representation for the nuclear spins so that the nuclear spin operators are retained as operators. One finds

$$\mathcal{H}_e = g_n\mu_n H_e(I_{zT}) + Q_0(I_{1z} - I_{2z})^2 + D_n[I_{1z}^2 + I_{2z}^2 - I_1(I_1+1) - I_2(I_2+1)] + J_n(I_1I_2 - I_{1z}I_{2z}), \quad \text{(A2)}$$

in which all of the parameters are functions of S_T and M_T defined as follows:

$$g_n\mu_n H_e = -g_n\mu_n H_Z + \tfrac{1}{2}AM_T + P_- + Q_- - P_+ - Q_+ , \quad \text{(A3)}$$

$$Q_0 = (\tfrac{1}{2}A)^2 \sum_{S_T'}{}' \frac{|\langle S_T, M_T|(S_{1z} - S_{2z})|S_T' M_T\rangle|^2}{E_{S_T,M_T} - E_{S_T',M_T}} , \quad \text{(A4)}$$

$$D_n = P_+ + P_- + Q_+ + Q_- , \quad \text{(A5)}$$

$$J_n = 2(P_+ + P_- - Q_+ - Q_-) \quad \text{(A6)}$$

and

$$P_\pm = \left(\frac{A}{4}\right)^2 \frac{|\langle S_T, M_T|(S_{1\pm} + S_{2\pm})|S_T, M_T \mp 1\rangle|^2}{E_{S_T,M_T} - E_{S_T,M_T\mp1}} , \quad \text{(A7)}$$

$$Q_\pm = \left(\frac{A}{4}\right)^2 \sum_{S_T'}{}' \frac{|\langle S_T, M_T|(S_{1\pm} - S_{2\pm})|S_T', M_T \mp 1\rangle|^2}{E_{S_T,M_T} - E_{S_T',M_T\mp1}} . \quad \text{(A8)}$$

The sums shown with a prime are over states with S_T' differing by ±1 from S_T.

Straightforward perturbation theory in a product representation for the nuclei will reproduce all of the terms in (A2) except the last one, the pseudonuclear spin-spin interaction. For the Mn X-X pairs to which we have applied (A2), $J_n/g\mu_B \simeq 1.0$ G for both the 5, −5 and 5, −4 electronic levels. The energy denominators in (A4)–(A8) were corrected for the effects of $D(X)$ and third order hyperfine corrections were included. It should also be noted that accuracy of the Q_0 term is dependent on the approximation $J \gg A$.

*Work supported in part by NSF Grant No. GH-34582. Helium gas supplied by Office of Naval Research Contract No. NOnr-2775(00).

†Present address, Department of Physics, Indiana University, Bloomington, Ind.

[1]J. W. Culvahouse and David P. Schinke, Phys. Rev. 187, 671 (1969).

[2]J. W. Culvahouse, D. P. Schinke, and Larry G. Pfortmiller, Phys. Rev. 177, 454 (1969).

[3]R. T. Dixon and J. W. Culvahouse, Phys. Rev. B 3, 2279 (1971).

[4]C. L. Francis and J. W. Culvahouse, AIP Conf. Proc. 10, 1044 (1972).

[5]This facility is a part of real-time computer network development supported in part by NSF Grant No. GJ-32213.

[6]K. W. Mess, E. Lagendijk, N. J. Zimmerman, A. J. Van Duyneveldt, J. J. Giesen, and W. J. Huiskamp, Physica 43, 165 (1969).

[7]Allan Zalkin, J. D. Forrester, and David H. Templeton, J. Chem. Phys. 39, 2881 (1963).

[8]S. Geschwind, Phys. Rev. 121, 363 (1961).

[9]Dirk Van Ormondt, Ph.D. dissertation (Delft, Netherlands, 1968) (unpublished).

[10]Melvyn J. Marple and J. W. Culvahouse, IEEE Trans. Nucl. Sci. NS-22, 502 (1975).

[11]R. W. Wilkins, D. G. Baldwin, H. W. Glotfelty, and J. W. Culvahouse, Bull. Am. Phys. Soc. 20, 387 (1975).

[12]C. P. Slichter, Phys. Rev. 99, 479 (1955).

[13]The operators O_4^0 are the Stevens operators, which are used in standard texts. The nondiagonal terms involving operators O_4^3 require the more general notation of R. J. Birgeneau [Can. J. Phys. 45, 3761 (1967)]. These terms are unimportant for the purpose of this section and have been omitted in Eq. (6).

[14]The second-order effects of the hyperfine interaction were ignored in Ref. 2, because they were absent in one and negligible in the other of the two cases investigated there. There are two misprints on p. 456 of that paper. The denominator of Eq. (13c) should include a $-p$, and a term $-\frac{1}{2}AM$ is missing from Eq. (16c).

[15]This result was calculated using the Fourier-transform method described by F. W. de Wette and G. E. Schacher [Phys. Rev. 137, A78 (1965)].

[16]R. C. Sapp and D. A. Nelson, Bull. Am. Phys. Soc. 11, 911 (1966).

[17]W. P. Wolf and J. F. Heintz, J. Appl. Phys. 36, 1127 (1965).

[18]R. C. Sapp (private communication).

[19]T. E. Feutchwang, Phys. Rev. 126, 1616 (1962).